Trigonal Boracites - A New Type of Ferroelectric and Ferromagnetoelectric that Allows no 180° Electric Polarization Reversal

Schmid, Hans

How to cite

SCHMID, Hans. Trigonal Boracites - A New Type of Ferroelectric and Ferromagnetoelectric that Allows no 180° Electric Polarization Reversal. In: Physica status solidi. B, Basic research, 1970, vol. 37, n° 1, p. 209–223. doi: 10.1002/pssb.19700370125

This publication URL: https://archive-ouverte.unige.ch/unige:32931
Publication DOI: 10.1002/pssb.19700370125

phys. stat. sol. **37**, 209 (1970)

Subject classification: 14.4.2; 1.2; 3; 4; 18.2

Battelle Institute, Geneva Research Centre, Geneva

Trigonal Boracites — A New Type of Ferroelectric and Ferromagnetoelectric that Allows no 180° Electric Polarization Reversal[1])

By

H. SCHMID

The space group of the trigonal phase of the Fe–Cl, Fe–Br, Fe–I, Co–Cl, and Zn–Cl boracites is established as C_{3v}^6. Ferroelectricity is evidenced by domain switching. High coercive fields at room temperature (up to 800 kV/cm) are found. Polarization-microscopical studies show that the polarization vector is not reversible by 180° but can jump only from, e.g., $[\bar{1}\bar{1}\bar{1}]$ to $[11\bar{1}]$, $[1\bar{1}1]$, or $[\bar{1}11]$, etc., in accord with crystal structure and group theoretical symmetry considerations. Two twinning "laws" are observed: a) head–head (tail–tail) domains with $\{110\}_{cub}$ as composition plane and b) head–tail domains with $\{100\}_{cub}$ as composition plane. The domain structure and the relevant twinning operations are discussed. The onset of ferromagnetism at low temperature in Fe–Cl, Fe–Br, Fe–I, and Co–Cl boracites leads to ferromagnetoelectricity. In the case of Co–Cl boracite the ferromagnetoelectric point group is m.

Die Raumgruppe der trigonalen Phase der Fe–Cl-, Fe–Br-, Fe–I-, Co–Cl- und Zn–Cl-Borazite wurde zu C_{3v}^6 bestimmt. Ferroelektrizität wird durch Bereichumklappung nachgewiesen. Die Koerzitivfelder bei Zimmertemperatur sind sehr hoch (bis zu 800 kV/cm). Polarisationsmikroskopische Studien zeigen, daß der Polarisationsvektor nicht um 180° umklappbar ist, sondern nur von z. B. $[\bar{1}\bar{1}\bar{1}]$ nach $[11\bar{1}]$, $[1\bar{1}1]$ oder $[\bar{1}11]$ usw. springen kann. Dies steht in Übereinstimmung mit der Kristallstruktur und Symmetriebetrachtungen. Zwei Zwillings„gesetze" treten auf: a) Kopf–Kopf (Schwanz–Schwanz)-Bereiche mit $\{110\}_{cub}$ und b) Kopf–Schwanz-Bereiche mit $\{100\}_{cub}$ als Verwachsungsebene. Die Bereichstruktur und die entsprechenden Zwillingsoperationen werden besprochen. Das Auftreten von Ferromagnetismus bei tiefen Temperaturen führt bei Fe–Cl-, Fe–Br-, Fe–I- und Co–Cl-Boraziten zu Ferromagnetoelektrizität. Co–Cl-Borazit hat die ferromagnetoelektrische Punktgruppe m.

1. Introduction

The structure family of boracites $Me_3B_7O_{13}X$ (Me bivalent metal ion, X = Cl, Br, or I) has recently become of interest because one of its representatives — Ni–I boracite — has been found to be ferromagnetoelectric (i.e. simultaneously ferromagnetic and ferroelectric) with strong coupling between spontaneous polarization and magnetization [1, 2]. Fe–Cl, Fe–Br, Fe–I, Co–Cl, and Zn–Cl boracites were reported to display polymorphic transitions from cubic over orthorhombic to trigonal symmetry by decreasing the temperature [3]. This paper is intended to prove the ferroelectric character of the trigonal phases, to interpret by means of their crystal structure the peculiar switching behaviour of the domains, and to show that some of these phases — reported as ferromagnets [4] — necessarily must become ferromagnetoelectrics below their Curie temperatures.

[1]) Work supported by the Battelle Institute, Geneva Research Centre (Physics Department).

2. Structural Aspects

2.1 Morphology and sample preparation

The investigated crystals were obtained by gas-phase transport [5]. They had natural (100), (110), and (111) facets as described for the Ni–I boracite [2]. Only small crystals (1 to 4 mm diameter) were crack-free and adequate for measurements. After X-ray or morphologic orientation, the crystals were cut by a diamond saw, ground on SiC paper, and polished with diamond paste (down to 0.25 μm diamond grain size).

2.2 Space group and unit cell

Weissenberg CuK_α photographs were made on a single domain (0.4 mm^3) that was cut of an as-grown Fe–Cl boracite crystal. The extinction laws were compatible only with space groups D_3^6 and C_{3v}^6. The former is ruled out by multiple reasons (ferroelectric switching, etc.), hence C_{3v}^6 (R3c) is the correct space group. This result agrees with the group theoretical prediction based on Ascher's selection rules of maximal polar subgroups [6, 7]: the only trigonal equi-translation subgroup of T_d^5 ($F\bar{4}\,3c$) being maximal and polar, and which should hence designate the ferroelectric symmetry, is C_{3v}^6. Furthermore, the extinction laws show that the smallest trigonal cell corresponds to the primitive trigonal cell of the face-centred cubic phase (Fig. 1). Therefore, in boracites, C_{3v}^6 is really an equi-translation subgroup of T_d^5, thus fully satisfying Ascher's rule. Hilti [8] has confirmed the space group C_{3v}^6 for the Fe–Cl boracite by precession photographs (Mo radiation) and has found the Fe–Br, Co–Cl, and Zn–Cl boracites to be isotypic. There is evidence from Mössbauer effect data [3] that Fe–I boracite is also isotypic.

2.3 Lattice parameters

In Table 1, we give the lattice parameters of some trigonal boracites as determined by Hilti [8] by means of Jagodzinski and de Wolff diagrams. The spontaneous strains relative to the cubic phase are very small. While the Zn–Cl boracite is elongated along $\boldsymbol{P}_s$, the Fe–Cl and Fe–Br boracites are compressed along that direction (Fig. 2). A magnetostrictive contribution of the paramagnetic ions to the spontaneous strain may account for the opposite behaviour. The trigonal splitting of the Co–Cl boracite was not resolved.

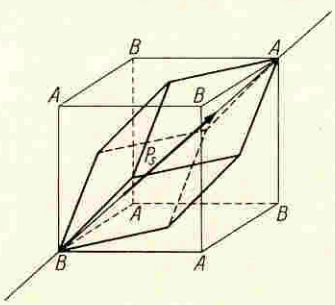

Fig. 1. Trigonal unit cell in the framework of the cubic high-temperature unit cell (trigonal cell ≡ primitive cell of cubic f.c. phase)

Table 1

Lattice parameters (refined by the least-squares method) of three rhombohedral boracites (25 °C, CuK_α radiation [8])

Boracite	Smallest hexagonal cell		Smallest rhombohedral cell		Pseudo-cubic rhombohedral cell	
	a_H (Å)	c_H (Å)	a_R (Å)	α	a'_R (Å)	α'
Fe–Cl	8.6240 ± 0.0002	21.0489 ± 0.0007	8.6036 ± 0.0002	60°09′56″	12.1817 ± 0.0003	90°08′12″
Fe–Br	8.6339 ± 0.0004	21.1004 ± 0.0014	8.6208 ± 0.0004	60°06′02″	12.2009 ± 0.0005	90°05′14″
Zn–Cl	8.5367 ± 0.0002	20.9722 ± 0.0007	8.5535 ± 0.0002	59°52′12″	12.0846 ± 0.0003	89°53′16″

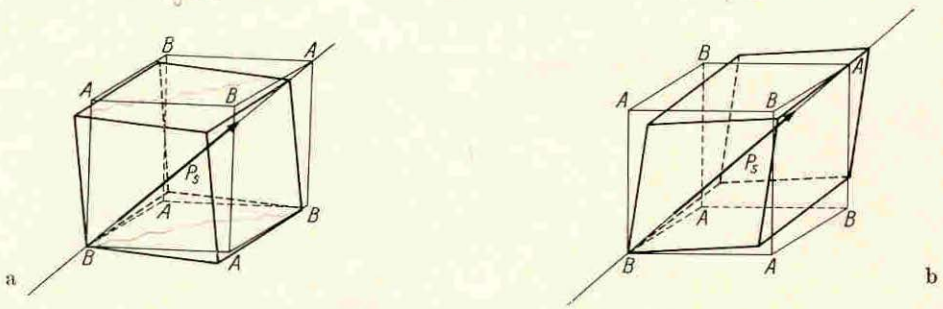

Fig. 2. Pseudo-cubic trigonal cell. a) Compressed along $\boldsymbol{P}_s$; b) elongated along $\boldsymbol{P}_s$

2.4 Ferroelectric switching

2.4.1 Particularities of the transition from T_d^5 *to* C_{3v}^6

Because the [111] directions of T_d^5, the "mother" phase of C_{3v}^6, are already polar (owing to the boron–oxygen net), it becomes clear that 180° domain reversal should be impossible in the trigonal boracites. However, domain "jumping" could be expected between the four preferential directions — $[\bar{1}\bar{1}\bar{1}]$, $[11\bar{1}]$, $[1\bar{1}1]$, and $[\bar{1}11]$ — of $\boldsymbol{P}_s$ (Fig. 3). For the general case, Ascher [9] has shown by group theory how to determine those ferroelectrics for which $\boldsymbol{P}_s$ has different directions but cannot be reversed: it is necessary to determine a) the number of C conjugates in the paraelectric (high-temperature) symmetry group H of a given subgroup G_i, and b) the index I of G_i in H. Then, either $I = C$ or $I = 2\,C$. In the former case, there exist C different orientations of $\boldsymbol{P}_s$ that cannot be reversed; in the latter one the number of $\boldsymbol{P}_s$-orientations is the same but their vector can be reversed. Aizu [10] has classified all possible pairs of high-temperature/low-temperature symmetry that lead to ferroelectrics with an "irreversible but divertible" polarization vector.

2.4.2 Sample preparation

Platelets (20 to 100 μm thick) of the Fe–Cl, Fe–Br, Co–Cl, and Zn–Cl boracites were cut parallel $(111)_{cub}$. For domain switching, these samples were mounted on a sample holder, which is schematically shown in Fig. 4: the crystal (e) was mounted by means of a resin (d) above the cone-like hole (0.3 to 2 mm diameter) of a Resocell plate (f). The electrodes (a) were painted with silver paste close to the crystal on the Resocell. Droplets of salt water solution (LiF) (b)

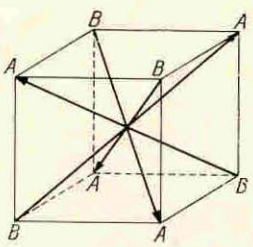

Fig. 3. The four possible directions of the spontaneous polarization in the C_{3v} boracite phase

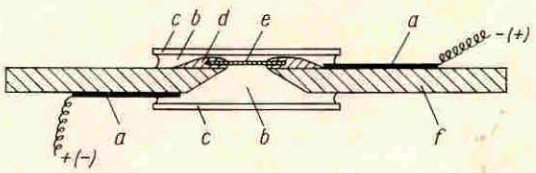

Fig. 4. Sample holder (schematic) for switching experiments with liquid electrodes and microscope observations

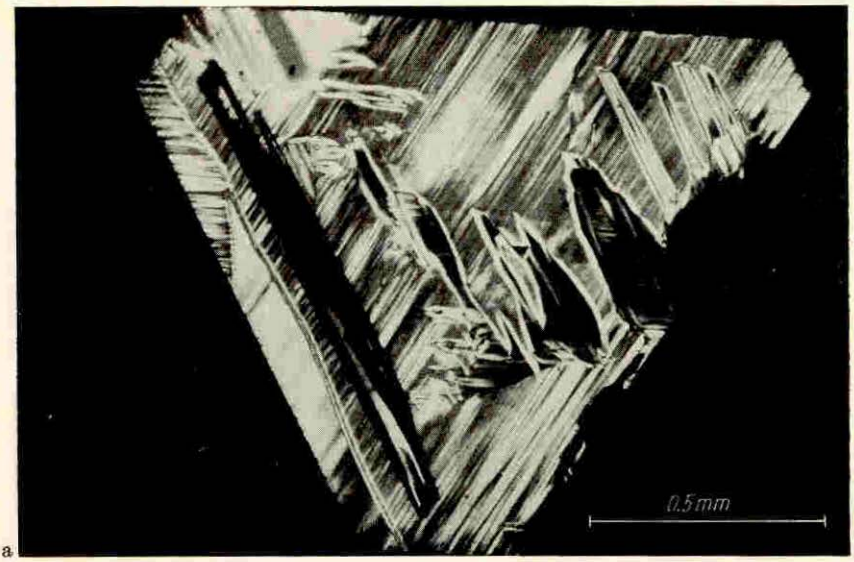

a

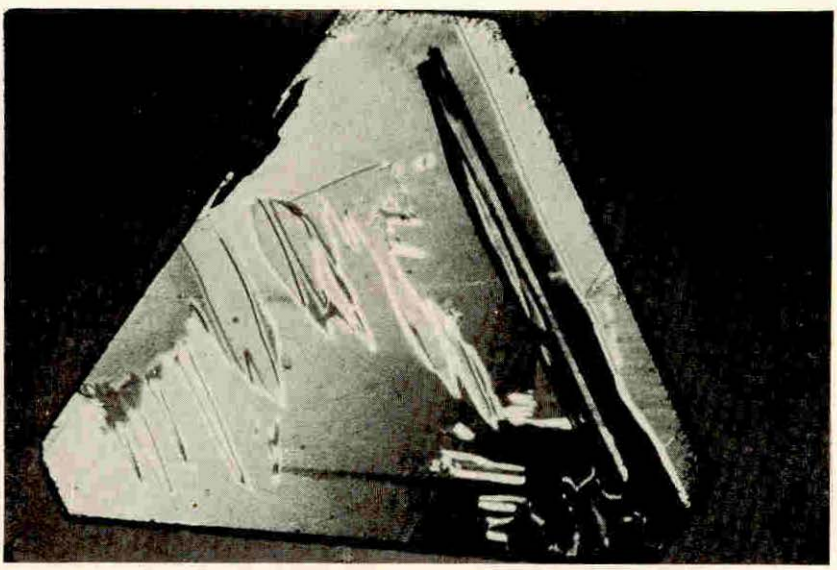

b

Fig. 5. a) Lamellar domain structure of the Zn–Cl boracite. C_{3v} phase, 25 °C, (111) cut; explanation on Fig. 13 Q/R. b) The same crystal in the C_{3v} phase, 350 °C

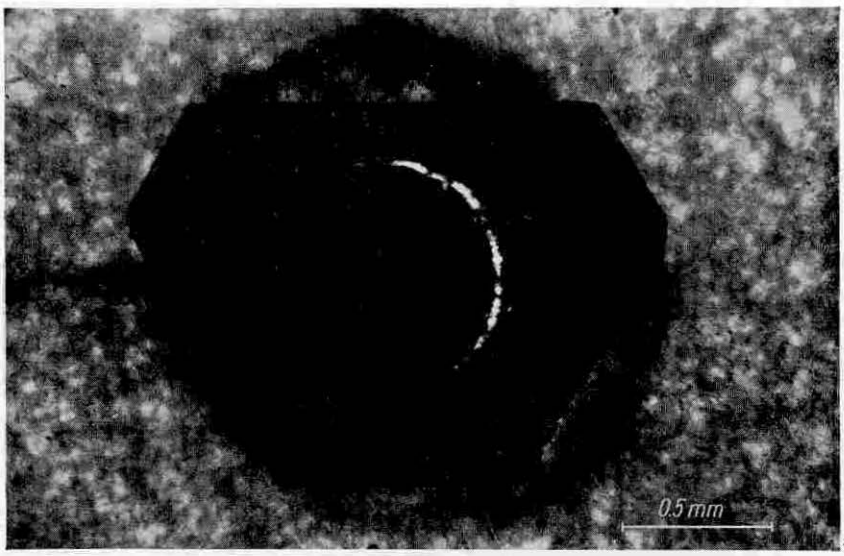

a

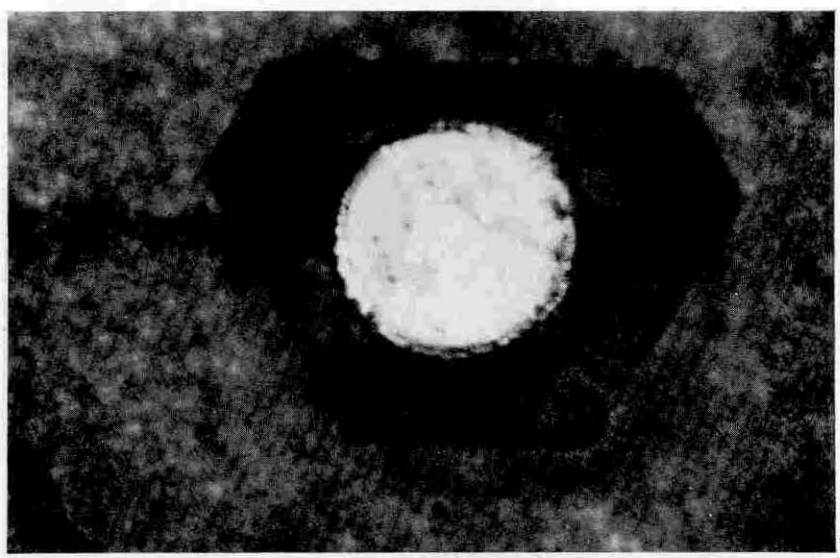

b

Fig. 6. Domain switching in the Co–Cl boracite, (111) cut, polarizers crossed. a) P_s perpendicular to platelet; b) domains of the three other preferential directions of P_s, all domains in non-extinction position

Fig. 6 c. Explanation to Fig. 6 b

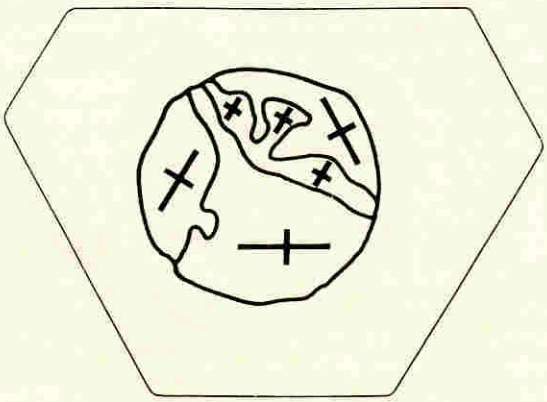

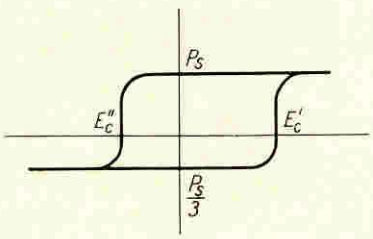

Fig. 7. Schematic asymmetric hysteresis loop as expected for C_{3v} boracites

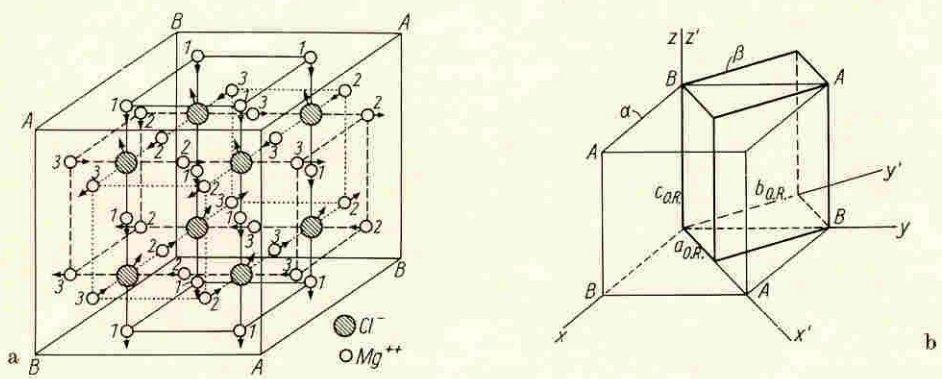

Fig. 8. The Me^{2+} and halogen displacements in the C_{3v} phase of the Mg–Cl boracite relative to the cell of the T_d-phase. Boron–oxygen skeleton not shown

provided the electrical contact between leads and crystal. To allow for good optical image quality, the droplets were stretched out by means of a cover glass adhering by capillary effect. The whole assembly was mounted on the gliding stage of a polarizing microscope. The adhering problem of the resin was crucial, particularly for the extremely high voltages applied. After trial of several products, a bee wax–colophony mixture (about 1:1) was found to meet best the requirements both of isolation and of a certain plasticity.

2.4.3 Results of switching experiments

The (111) platelets of the Fe–Cl, Fe–Br, Co–Cl, and Zn–Cl boracites could be switched at room temperature. The electric field strengths at which part of the domains began to move lay between 5 to 10 kV/cm, whereas those for saturation were found between 400 and 800 kV/cm. In Table 2, we give some typical values of the coercive fields. For most Co–Cl boracite crystals, the remanence was equal to saturation after saturation at 500 kV/cm, whereas for the other compositions, the remanence lay appreciably below saturation.

Table 2

Switching field strength of some trigonal boracites
(25 °C, (111) cut)

Boracite	Beginning (kV/cm)	Saturation (kV/cm)	Thickness of platelet (μm)
Fe–Cl	320	800	25
Fe–Br	50	75	107
Co–Cl	240	600	50
Zn–Cl	280		35

Closely related to the high coercive fields are the long switching times. For example, at 50 Hz and 800 kV/cm only about 1 to 5% of the domains of the Co–Cl boracite were optically observed to be in a state of switching (twinkling of colours between crossed polarizers); the remainder of the crystal was completely blocked. Therefore, very low frequency measurements are now being prepared to measure the spontaneous polarization and study the switching behaviour.

Before a trigonal as-grown and polished platelet is subjected to poling, it shows usually a very fine lamellar structure (Fig. 5a, explanation Fig. 13 Q/R). After repeated quasi-static switching, large domains are formed. The lamellar structure is reestablished only after heating above the transition temperature to cubic and cooling in zero field.

The photographs of Fig. 6 clearly demonstrate the domain "jumping" as seen in a (111) Co–Cl-boracite platelet. In Fig. 6a, the electric field polarity produced a single domain with the polarization direction and thereby the optical axis perpendicular to the platelet. The entire domain appears black between crossed polarizers. After reversal of the polarity of the field, the single domain splits up into the three remaining possible domain orientations, the polarization and optic axis directions of which form an angle of arctg $\sqrt{2}/2$ with the surface, their birefringences being correlated by a rotation of 120° (60°). Hence, at an adequate intermediate position of the crossed polarizers, there is contrast be-

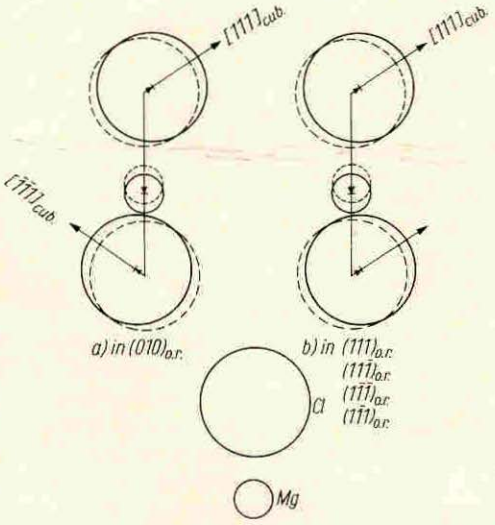

Fig. 9. The two kinds of Me^{2+} environment in the C_{2v} boracite. $(110)_{cub}$ cut, ion shifts in the plane of the paper.
a) Me^{2+} type 1 (1/3 of Me^{2+} ions);
b) Me^{2+} types 2 and 3 (2/3 of Me^{2+} ions)

tween all three domain categories (Fig. 6b and c). One can expect that for such crystal sections, the hysteresis loop will be asymmetric both in spontaneous polarization and in coercive field (Fig. 7).

2.5 Structure model and absolute configuration

The phase C_{2v}^5 of Mg, Ni, etc., -boracites is characterized by the presence of three crystallographically inequivalent Me^{2+} sites, 1, 2, and 3 (reference [11] and Fig. 8). Categories 2 and 3 have identical local environment (Fig. 9b); that of kind 1 (Fig. 9a) is quite different, leading to another electric field gradient at the metal site. Hence, there are two kinds of quadrupole splitting in the Mössbauer spectrum [3]. During the transition to the trigonal phase, only one kind of splitting survives. Because it evolves out of the splitting due to sites 2 and 3 with nearly no discontinuity at the phase transition, one can conclude that only one type (namely that of Fig. 9b) of local metal environment occurs in the trigonal phase. On the basis of this information and the space group requirements for C_{3v}^6, it turns out that only one kind of structure model is compatible with a polar axis along a cubic space diagonal [3, 12]. In Fig. 10 are represented the shifts of the metal and halogen ions with respect to the unit cell of the cubic phase T_d^5: all halogen ions move parallel to the direction of spontaneous polarization [111], whereas the metal ions move along $[100]_{cub}$ direc-

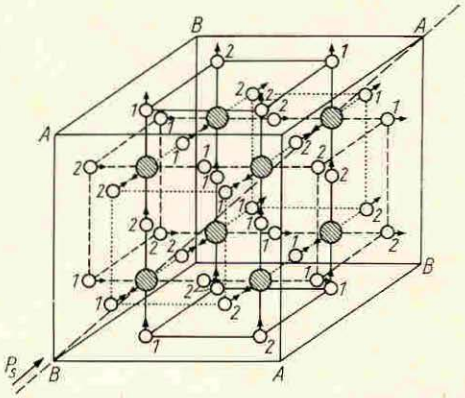

Fig. 10. Me^{2+} and halogen shifts in the C_{3v} phase relative to positions in the T_d-phase

tions as in the orthorhombic phase, their centre of gravity shifting oppositely to the displacement of the halogens. Recent structure work supports this model [13].

Inspection of the available space around the halogen (point symmetry T-23) in the cubic structure T_d^5 shows that there is ample space for the halogens to move in the [111] directions only towards the B-faces[2]) (Fig. 11). There is much less space in the direction towards the A-facets. In other words, there exists a saddle-like potential distribution, the (110) sections of which we have schematically represented in Fig. 12. The absolute configuration of the orthorhombic phase C_{2v}^5 and the cubic phase T_d^5 of the Ni–Cl boracite had been determined by a procedure combining pyroelectric, polarization-optical, X-ray-Weissenberg (without using anomalous dispersion!), and etching data [2]. (Independently thereof Abrahams et al. [14] used the pyroelectric effect in a similar manner for the determination of the absolute configuration of $LiNbO_3$.) The problem of the absolute configuration of the trigonal phase of boracites, based on the above-mentioned model, can be solved in a much simpler way than for the orthorhombic phase: The contribution to the spontaneous dipole moment resulting from the very small deformation of the boron–oxygen skeleton will be negligible relative to that caused by the shifts of the halogen and metal ions which are of the order of 0.1 Å [11]. It is clear from spatial considerations that the internal dipole moment (owing to the halogen and metal ion shifts) must point from the B- to the A-corner, if we define its direction conventionally by $- \rightarrow +$. In order to determine now the A, B (111) facets of a real crystal, we can do this by poling a thin (111) platelet (see above, Section 2.4). Then the polarity of the electrodes, which produces a single domain (or the triple

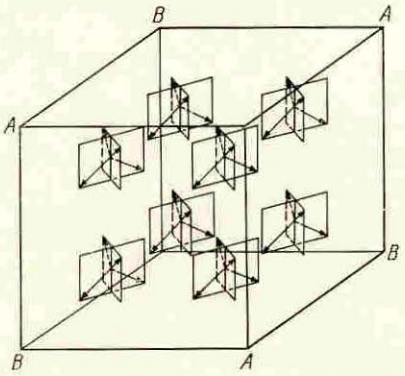

Fig. 11. Representation of the possible [111] directions of movement of the halogen ions

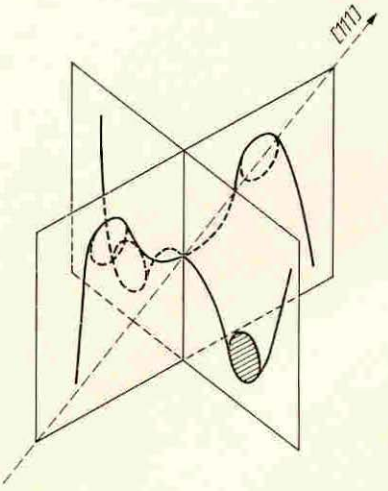

Fig. 12. Schematic representation of the (110) section through the saddle-like electrostatic potential of the halogen environment

[2]) We have defined the A-corners as those corners where a boron tetrahedron with an oxygen in its centre points with one of its corners *into* the unit cell. The A-corner is identical with the origin of Ito's unit cell setting [11].

domain configuration), indicates the A–B facets (cf. Fig. 10). We have made these experiments for the Co–Cl and Zn–Cl boracites and correlated the results with the orientation of the etch pits on the (100) facets. We can formulate the outcome in the rule: "The long axis of the etch pit rhomb of a boracite (100) facet always points to adjacent (111) B-facets." This result is in accord with the independently determined absolute configuration of cubic boracite via the orthorhombic phase [2]. In the case of the Co–Cl boracite, the (111) B-facets are nearly always larger than the A-facets. However, the situation is often reversed, or there is no difference in size at all (e.g., for the Fe boracites, etc.). Therefore, poling or etching gives the most reliable determiation of the absolute configuration of a boracite crystal. The form of the strain field of a growth centre, reported for the Ni–I boracite (100) growth sectors [2], is very reliable too; however, it has been found useful so far only for diagnostic purposes in that composition.

3. Twinning Laws

3.1 General aspects

By group theoretical and stuctural considerations it was shown (Sections 2.4.1 and 2.5) that there are four possible domain orientations with only four polarization directions in the C_{3v} phase of boracite (Fig. 3). These different domains are related by twinning operations that are given by the lost symmetry elements of the C_{3v} phase relative to the high-temperature "mother" phase T_d [9]. These are: 3 triads [111], 3 inversion tetrads [100], and 3 symmetry planes (110).

We have observed two kinds of composition plane, (100) and (110), between the rhombohedral domains. The first kind leads to head–tail and the second to head–head (tail–tail) configurations.

Both laws are often found in one and the same crystal.

3.2 Head–tail domains

The most frequent domain pattern consists of lamellas (thickness $\lesssim 1$ μm) of head–tail configurations with (100) as composition plane (Fig. 5, 13 R, and 14). Small crystals and thin platelets often show only *one* of these three mutually perpendicular possible orientations of layer piles (one of the three sets of pile is shown in Fig. 13 O/R a, 14 and two in Fig. 16), because such an arrangement can be free of constraints. The head–tail layers are favourable because they minimize the electrostatic energy by preventing "space charges" on the interfaces. This explains their appearance in highly isolating crystals as separation walls between the three equivalent domains of a $(111)_{cub}$ platelet (Fig. 6 b, c); however, frequently strong angular deviations from $(100)_{cub}$ were observed.

3.3 Head–head (tail–tail) domains

Much less frequently than head–tail domains, the head–head (tail–tail) junctions are observed (Fig. 13 S). This configuration creates "space charges" on the composition planes, since div $\boldsymbol{P}$ is not zero. It is obvious that this kind of twinning will occur more easily in conducting than in highly insulating crystals. In Fig. 15 a rare example of a large head–head boundary is shown.

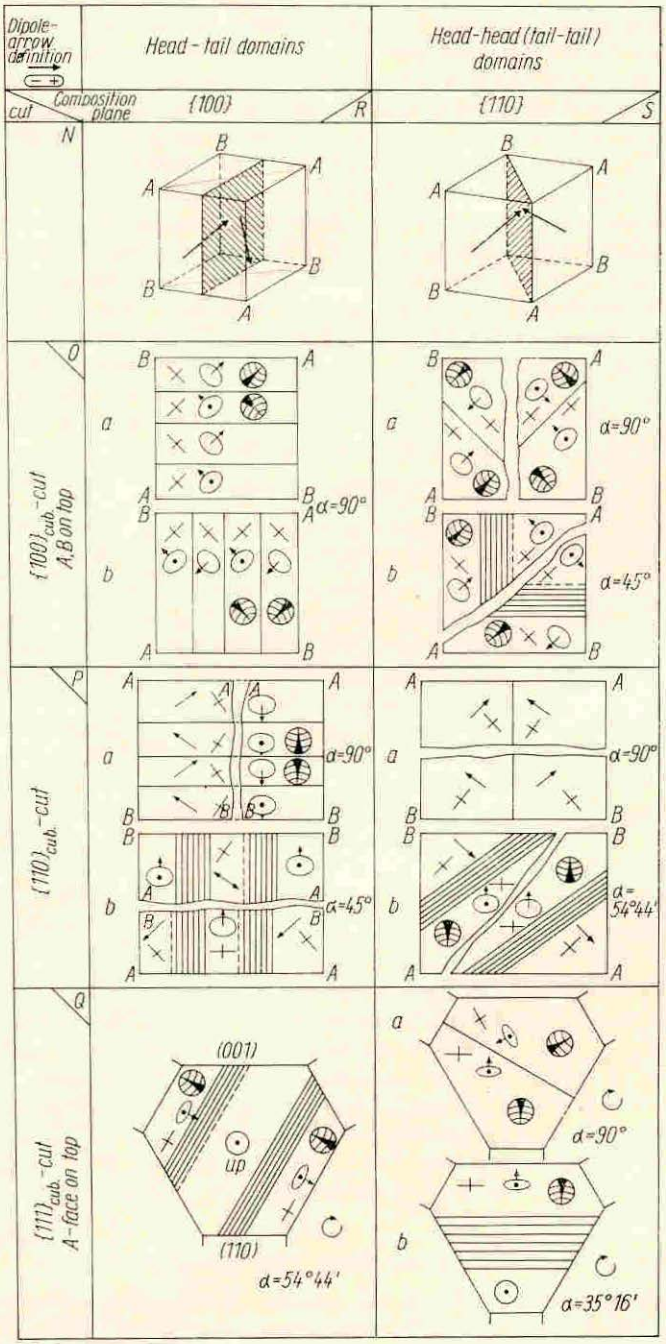

Fig. 13. Schematic representation of head–head and head–tail domains as seen on $(100)_{cub}$, $(110)_{cub}$, and $(111)_{cub}$ cuts

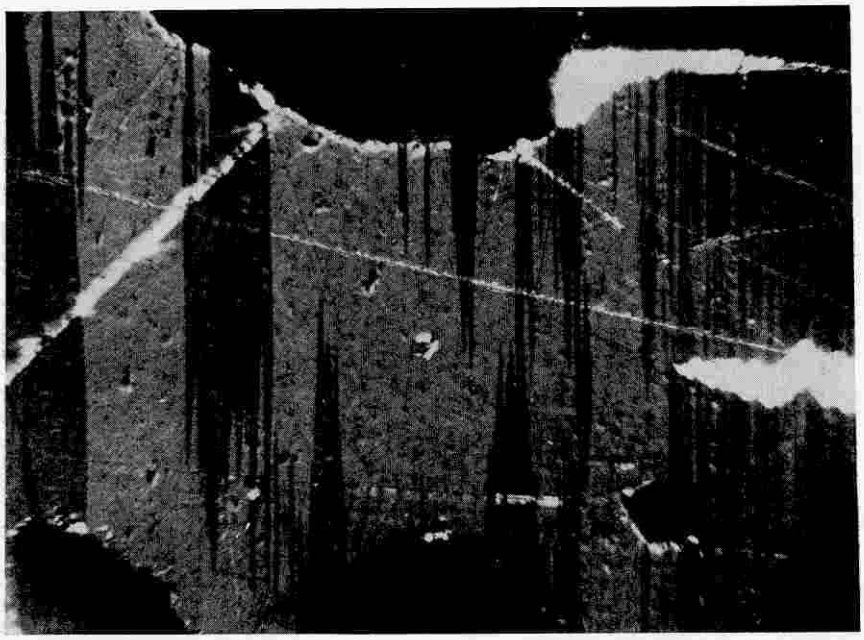

Fig. 14. Head–tail domains on a $(110)_{cub}$ cut (thickness 28 μm) of the Fe–Cl boracite

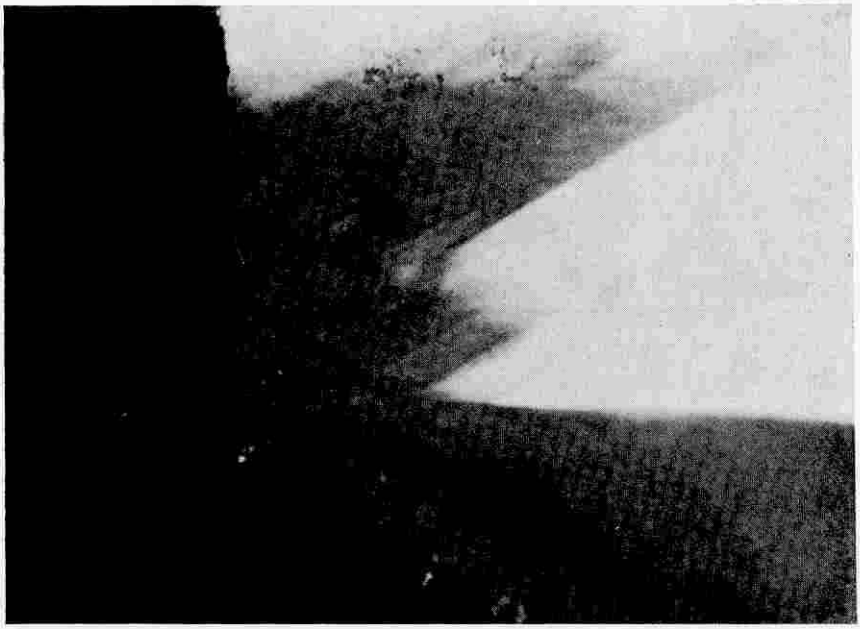

Fig. 15. Large head–head domains of the Fe–Cl boracite, $(111)_{cub}$ cut (explanation on Fig. 13 Q/S)

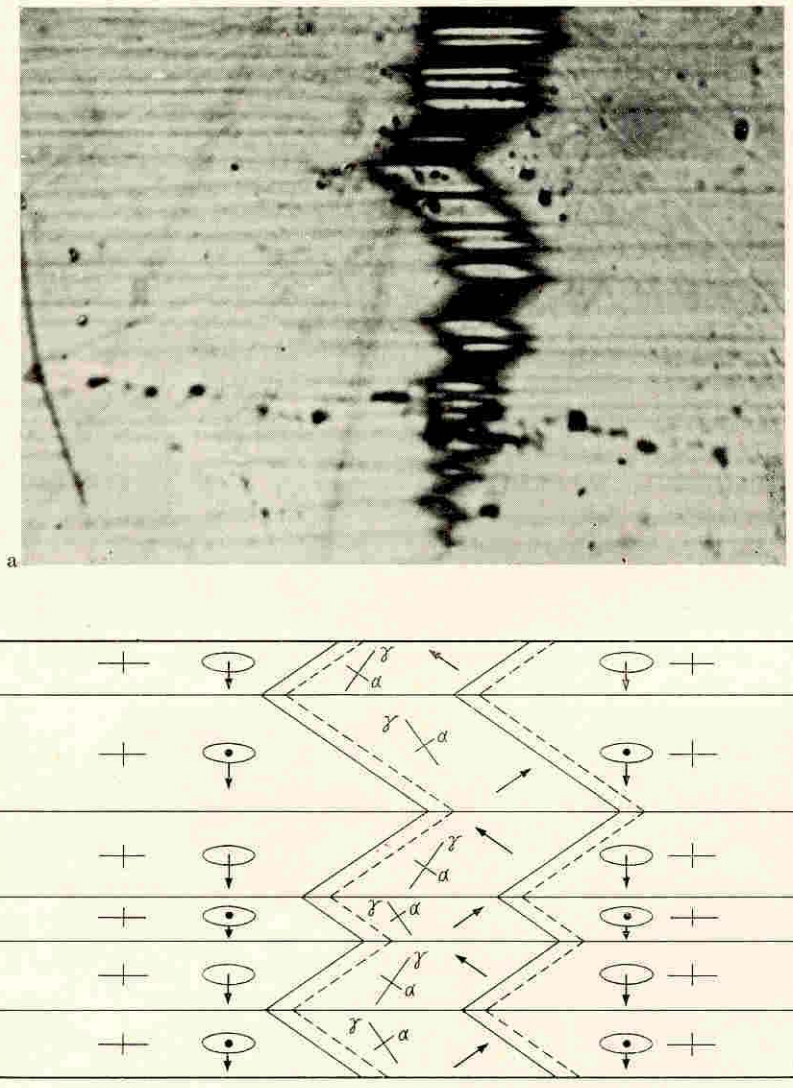

Fig. 16. Linking of two sets of head–tail lamellas by head–head domains, (110) cut, of Fe–Cl boracite. a) Real; b) schematic

If all four polarization directions are present in one and the same crystal, usually two or three mutually perpendicular sets of head–tail lamellas appear. The different sets are then joined by head–head (tail–tail) composition planes. This is shown in Fig. 16a for a (110) cut of the Fe–Cl boracite and is schematically explained in Fig. 16b. The juxtaposition of these two kinds of twinning must create mechanical constraints, but since the deviations from cubic symmetry are extremely small (see reference [15] and Table 1), the arrangement becomes comprehensible.

4. Remarks on Ferromagnetoelectricity

Magnetic measurements have shown [4] that the trigonal phases of the Fe–Cl, Fe–Br, Fe–I, and Co–Cl boracites become ferromagnetic below 11.5, 15, 30, and 15 °K, respectively. In the case of Co–Cl boracite it could be shown by observation of the Faraday effect that the spontaneous magnetization lies perpendicular to the spontaneous polarization of the 3 m 1′ paramagnetic phase. Combining this result with magnetoelectric measurements [17], we find the Shubnikov point group m, which is compatible with the coexistence of ferroelectricity and ferromagnetism. This symmetry allows the linear and high-order magnetoelectric effects ($\alpha_{ij} E_i H_j$, $\alpha_{ijk} H_i E_j E_k$, $\beta_{ijk} E_i H_j H_k$ [16]). Strong ferromagnetic-ferroelectric coupling is expected as occurring in $Ni_3B_7O_3I$. The linear magnetoelectric effect should lead to a "butterfly" loop as in $Ni_3B_7O_{13}I$ [2].

Acknowledgements

It is a pleasure to thank Dr. E. Ascher for helpful discussions, Dr. E. Hilti for providing lattice parameter data, H. Baier for taking the Weissenberg-photographs, and H. Tippmann for the careful preparation of single crystals.

References

[1] E. Ascher, H. Rieder, H. Schmid, and H. Stoessel, J. appl. Phys. **37**, 1404 (1966).
[2] H. Schmid, Acta cryst. **21**, (Suppl.) A263 (1966) (abstract); Rost Kristallov **7**, 32 (1967) (full text).
[3] H. Schmid and J. M. Trooster, Solid State Commun. **5**, 31 (1967).
[4] G. Quezel and H. Schmid, Solid State Commun. **6**, 447 (1968).
[5] H. Schmid, J. Phys. Chem. Solids **26**, 973 (1965).
[6] E. Ascher, Phys. Letters (Netherlands) **20**, 352 (1966).
[7] E. Ascher, Lattices of Equi-Translation Subgroups of the Space Groups, Battelle Institute, A.S.C., Geneva 1968 (available on request).
[8] E. Hilti, private communication (ETH Zürich; to be published).
[9] E. Ascher, private communications (to be published). — Material concerning the relations between phase transitions and symmetry is contained in the following documents by E. Ascher, which may be obtained on request: "A propos de ferromagnéto-électricité" (Conf. Neuchâtel, June 1966); "Symétrie et changements de phase continus" (Conf. Geneva, May 1967), "Group-Theoretical Considerations on Ferro-Electric Phase Transitions and Polarization Reversals" (Conf. Prague, May 1968), "Relations entre structure et propriétés — exemple des boracites" (Conf. Strasbourg, September 1968).
[10] K. Aizu, J. Phys. Soc. Japan **23**, 794 (1967).
[11] T. Ito, N. Morimoto, and R. Sadanaga, Acta cryst. **4**, 310 (1951).
[12] J. M. Trooster, Thesis, Nijmegen 1967; phys. stat. sol. **32**, 179 (1969).
[13] H. Schachner and H. Schmid, to be published.
[14] S. L. Abrahams, J. M. Reddy, and J. L. Bernstein, J. Phys. Chem. Solids **27**, 997 (1966).
[15] J. Kobayashi, N. Yamada, and T. Azumi, Rev. sci. Instrum. **39**, 1647 (1968).
[16] E. Ascher, Phil. Mag. **17**, 199 (1968).
[17] H. Schmid, to be published.

(Received August 20, 1969)